International Journal of Fatigue 190 (2025) 108642

Contents lists available at ScienceDirect

International Journal of Fatigue

journal homepage: www.elsevier.com/locate/ijfatigue

Monitoring of crack length growth on welded specimens by applying square wave inductive thermography

Paul Dario Toasa Caiza [a,*], Daiki Shiozawa [b], Yuya Murao [b], Thomas Ummenhofer [a], Takahide Sakagami [b]

[a] KIT Stahl- und Leichtbau, Versuchsanstalt für Stahl, Holz und Steine, Karlsruher Institut für Technologie (KIT), Otto-Ammann-Platz 1, 76131 Karlsruhe, Germany
[b] Department of Mechanical Engineering/Graduate School of Engineering, Kobe University, 1-1, Rokkodai-cho, Nada-ku, Kobe, 657-8501, Japan

ARTICLE INFO

Keywords:
Crack growth
Crack length
Crack detection
Monitoring
Real time
Active thermography

ABSTRACT

The crack growth monitoring is an important task for the maintenance policies of steel structures subjected to cyclic loading, such as bridges, cranes, off shore facilities and wind energy towers. A reliable crack detection method allows to survey properly the crack initiation and growth in responsive details of these structures, so that, they can be repaired or restored in time in order to avoid services interruption, accidents or structural collapses. In this paper, a crack detection system, which is based on inductive thermography is applied to survey the crack growth on a SM490 steel welded specimen subjected to cyclic loading. The required thermal excitation of this system is based on the generation of eddy currents, which cause a temperature increase on the crack tips. This temperature rise can be observed and recorded by using an infrared camera. Afterwards, the crack tip and growth are established by analysing the infrared (IR) images. The mentioned system allows to detect cracks on steel structures in real time and *in situ*, characteristics that represent the efficiency and the potential of this method in the field of NDT.

1. Introduction

The detection of cracks caused by cyclic loading in steel structures is an important issue to be taken into account in the monitoring protocols and maintenance policies. Failures induced by fatigue begin with the crack initiation and continue during the critical stage caused by the crack growth. For this reason, it is very important to have at disposal a reliable system, which detects the presence of cracks and monitors their growth as well. Problems with non-destructive testing of large steel structures such as bridges include the need to perform testing at high altitudes, to measure a wide area, and to remove anti-corrosive coatings. Therefore, we focused on the thermography method.

Several studies have been carried out using infrared thermography to study crack growth, applying thermoelastic stress analysis (TSA) to observe the crack propagation [1], evaluate the effect of mean stress in T-joints [2], and calculate stress intensity factors as a function of heat source from thermoelastic stress analysis around the crack tip [3,4] or analysing the case of delaminations in thermal barrier coatings [5].

Sakagami [6] proposed a method to detect weld cracks in bridges by utilizing changes in temperature distribution caused by fatigue cracks when the object is heated by the sun, and demonstrated that fatigue cracks in bridges can actually be detected. Such passive thermography methods have the problem of limitations on the measurement environment and inspection locations.

A typical active thermography method is a measurement technology that can inspect a wide area non-contactly without being affected by the surrounding environment, and can achieve high accuracy by modulating the external thermal load. In this study, induction heating by generating eddy currents was used as the heating method for the active thermography method [7]. Induction heating is effective when applied to magnetic materials such as steel. A short induction heating pulse induces eddy currents in the measurement object and an infrared camera records the surface temperature distribution. As cracks disturb the eddy current distribution and the heat diffusion, they become visible in the infrared images, see Fig. 1. The shorter the crack, the more complex the relationship between eddy current distribution and thermal diffusion becomes, so investigations are being conducted into detection conditions, such as excitation frequency and heating pulse duration, for short cracks [8].

Conventional induction heating thermography has a problem in that the coil temperature rises during inspection, which affects the detection of cracks. In addition, it requires large power supply and cooling

* Corresponding author.
E-mail address: paul.toasa@kit.edu (P.D. Toasa Caiza).

https://doi.org/10.1016/j.ijfatigue.2024.108642
Received 13 August 2024; Received in revised form 1 October 2024; Accepted 7 October 2024
Available online 16 October 2024

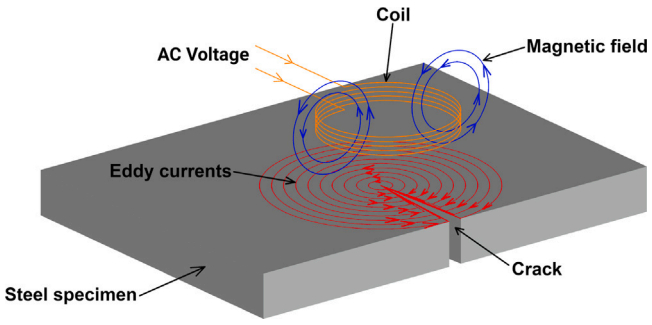

Fig. 1. Eddy currents generation.

Table 1
Coating properties.

Process	Painting	Thickness [μm]
Surface preparation	Blasting treatment ISO Sa $2\frac{1}{2}$	–
Anti-corrosion base coating	Inorganic zinc rich primer	75 ~ 90
Mist coat	Epoxy resin paint	–
Undercoating	Epoxy resin paint	50
Total thickness		125 ~ 140

devices, making it difficult to apply on large steel structures like bridges and high-altitude sites. Therefore, the authors developed an active thermography system that suppresses the temperature rise of the coil and can be significantly miniaturized, see Fig. 2. This is achieved by generating a square wave AC voltage from a DC voltage [9]. The square wave generation is performed by a control unit called: S2S[1] Hi Speed Wave Induction Unit.

This experimental setup has proven to be suitable for detecting cracks on the surface of steel structures under laboratory conditions and it also requires much less energy than the common systems [10]. Thus, this system is used to detect the cracks and monitor their growth in a coated welded steel specimen subjected to a cyclic loading.

First, the loading was launched up to reach the crack initiation in the welding toe. Afterwards, the loading continued to induce the crack growth on the horizontal steel plate. The loading was paused at preestablished number of cycles in order to perform the crack growth detection. The detection system is based on active thermography, whose thermal excitation is caused by the generation of eddy currents.

The subsequent sections of this paper are organized as follows: First, a detailed description of the experimental setup, which includes specimen properties and the loading procedure is presented. Afterwards, the crack growth monitoring during the cyclic loading is presented. This part includes a description of the active thermography system, the acquired IR images and the temperature variation at the crack tips. Then, based on the IR and microscopic images the crack growth, path and its length are established. Finally, the applicability of square wave inductive thermography to the evaluation of crack propagation under a coating is discussed.

2. Experimental procedure

In order to evaluate the suitability of the proposed NDT system based on square wave inductive thermography to perform a real time monitoring of the crack growth, a welded steel specimen with anti-corrosive coating was manufactured and subjected to a cyclic loading to induce the crack initiation at the weld toe. In this manuscript, the nucleation and micro crack propagation are considered as the crack

Fig. 2. Real time crack detection system. A: IR camera, B: coil, C: S2S unit, D: voltage supply, E: PC and F: steel specimen.

initiation phase, see [11,12]. Afterwards, the loading continued to induce the cracks growth on the horizontal plate at both sides of the weld toe. The loading was paused when preestablished loading cycles were reached in order to perform the crack detection and to measure its length by IR measurements and microscope.

2.1. Specimen

In this research, a SM490[2] steel specimen with a longitudinal stiffener welded with a convex fillet was used, see Fig. 3. The area where fatigue cracks initiate and propagate, including the weld toe, were coated with an anti-corrosion painting, see Fig. 3(a). Strain gauges for measuring the applied stress were attached to both sides of the specimen at the same longitudinal position as the weld toe. The composition and properties of the coating are described Table 1. Black paint was applied to improve reflectivity of the specimen surface.

2.2. Loading procedure, crack initiation and crack growth

An eccentric motor is attached to the steel specimen as shown in Fig. 4. By rotating the eccentric motor, resonant vibrations are generated, and a cyclic bending load is vertically applied to the plate as the arrow shows in Fig. 3(a). When the stress ratio is 0, the upper spring presses down on the specimen, and the stress on the top surface of the specimen is always in tension during vibration.

[1] S2S: Square to Shark.

[2] Japanese steel, whose grade is equivalent to S355J2 European steel.

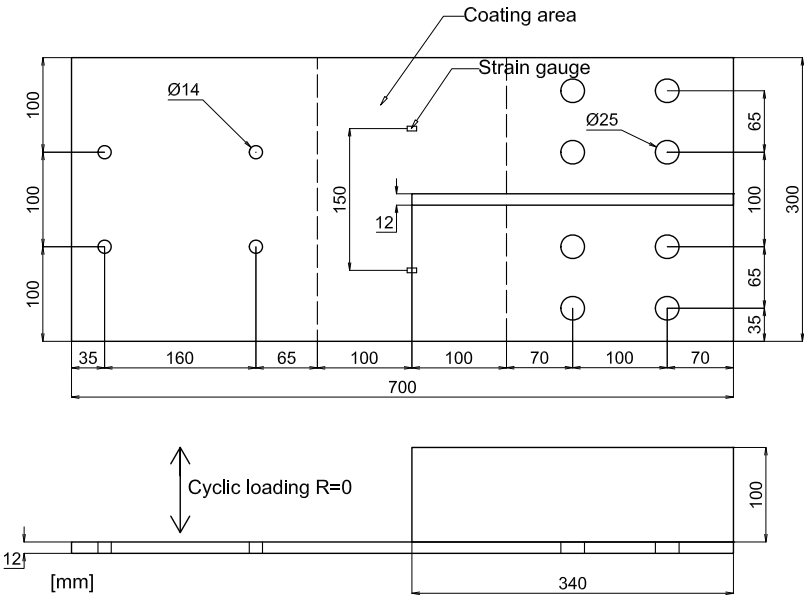

(a) Geometry.

(b) Specimen and coil.

Fig. 3. SM490 steel specimen.

Fig. 4. Cyclic loading machine.

The applied stress was calculated from the measurement results of the strain gauges. The strain gauge was attached to a location that was not affected by stress concentration due to the weld toe. The loading frequency was set to 18.1 Hz, the maximum applied stress to 80 MPa and the stress ratio to $R = 0$.

First, the bending load was applied up to N = 30 000 cycles, which induced the crack initiation and growth along the weld toe, as it is shown in Fig. 5.

Afterwards, on both sides of the weld toe, the crack length was measured on the surface of the plate. IR and microscopic images were used for this purpose. These images allowed to observe the cracks and establish the position of the crack tips after the loading, so that, the crack growth could be observed and measured.

This procedure was performed at eleven stages, starting at $N = 30\,000$ loading cycles and then resuming every $N = 50\,000$ loading cycles from $N = 100\,000$ up to $N = 550\,000$ cycles.

Fig. 6 shows a visible image of crack at $N = 550\,000$ loading cycles. It can be observed that the crack grows on both sides of the weld toe.

3. Real time crack growth monitoring with square-waveform inductive thermography

As it was mentioned in the previous Section 1, the active infrared thermography system proposed in this study does not require large power supplies and amplifiers, can suppress heat generation by the coil

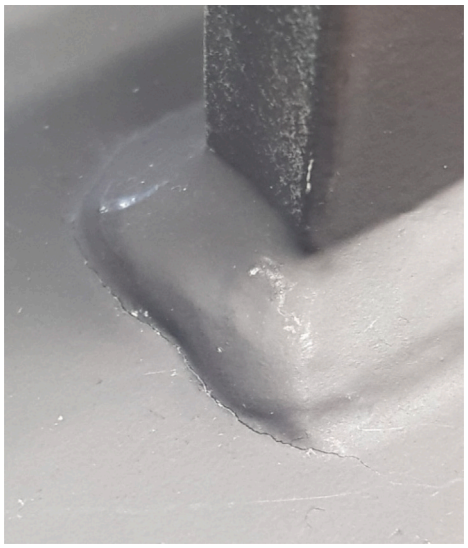

Fig. 5. Initial crack along the weld toe obtained after N = 30 000 loading cycles.

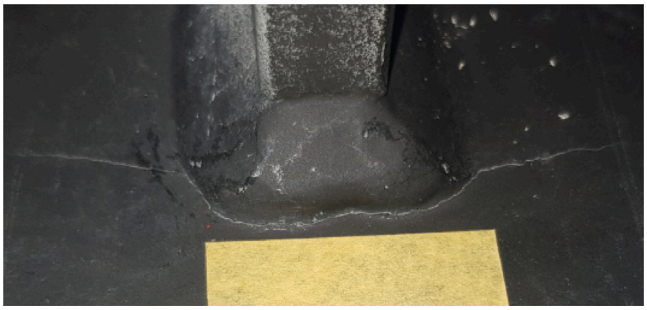

Fig. 6. Crack growth after N = 550 000 loading cycles.

itself, and offers the possibility of performing crack detection in real time on site at any time.

3.1. Active thermography system

The active thermography method applied for the monitoring of the crack growth is based on the eddy currents generated by inducing a high frequency AC voltage into a coil, see Fig. 1. In case that a crack is present on the surface of the specimen, the density of eddy currents increases on the edges of the crack. This fact causes a temperature rise in the edges of the crack. Finally, this thermal variation can be acquired with an IR camera. The block diagram of the corresponding system is shown in Fig. 7.

A detailed description of the NDT crack detection system is presented in [9,13,14] and its application in a similar geometry in [10]. Particularly, the experimental setup for the crack growth detection is shown in Fig. 8.

3.2. Infrared images and temperature evolution

As it was mentioned, IR images were taken after reaching a specific loading cycles during the fatigue test. Because of the temperature variation on the crack tips, these images describe clearly their location. In Fig. 9, some IR images of the right and left cracks at different loading cycles can be observed.

Since the IR images were obtained right after the cyclic loading, the low part of some images shows a higher temperature caused by the heat released from the loading machine motor.

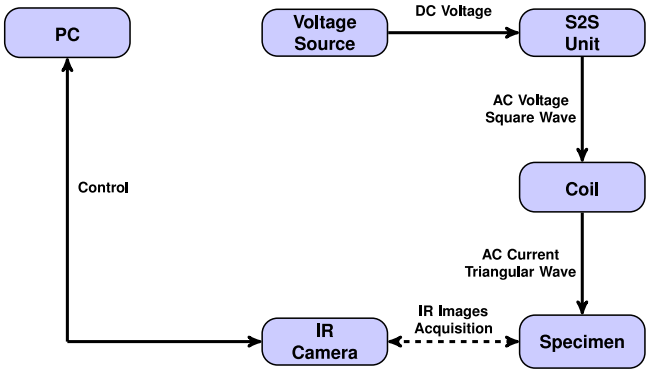

Fig. 7. Block diagram of the proposed experimental setup.

Fig. 8. Experimental setup during the crack growth monitoring.

The temperature evolution corresponding to the crack tips observed in Fig. 9 is shown in Fig. 10. These curves show the expected shark wave geometry corresponding to the temperature rise in the crack tip caused by eddy currents excitation, see [10]. The temperature rise on the coil or in other regions of the plate look completely different. The temperature peaks on the curves correspond to the moment, which is displayed in the IR images.

4. Crack path and length

By considering the IR and microscopic images obtained during the fatigue test, the crack growth rate and length can be established.

4.1. Results obtained from IR images

During the fatigue test, the cyclic loading was paused eleven times in order to acquire the IR images. The loading cycles corresponding to these pauses are shown in the Tables 2 and 3. The acquisition of IR images started at $N = 30000$ since, before that, the coil covered the region corresponding to the crack initiation. This is a limitation of the coil's geometry that hopefully can be overcome with better designs.

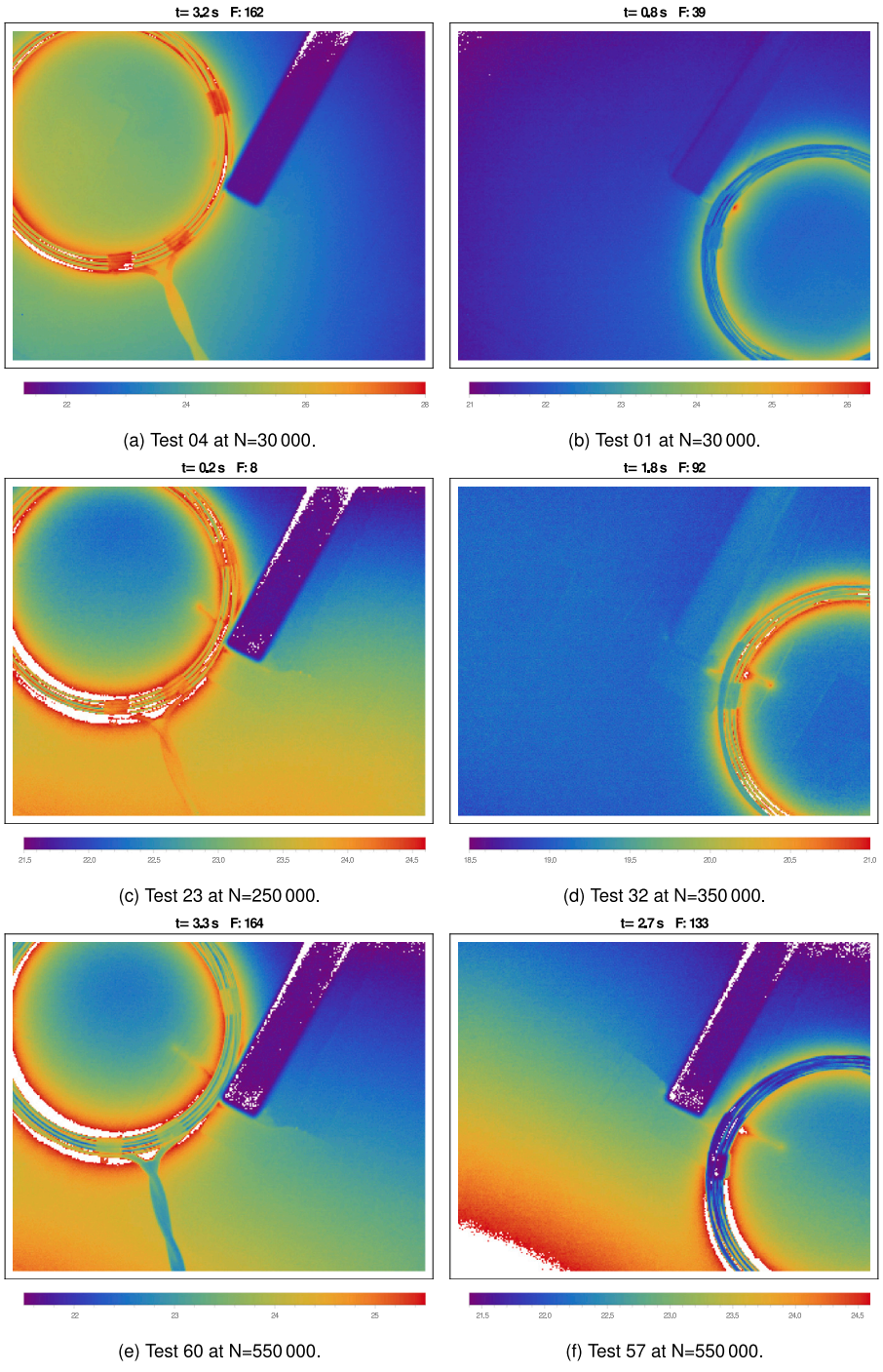

Fig. 9. Cracks growth from N = 30 000 to N = 550 000 loading cycles. The stiffener is seen in the upper right part and the coil creates a ring of temperature increase. The hot spot on the lower left corresponds to the heat dissipated by the loading engine.

The crack path can be plotted by considering the coordinates of the crack tips detected on the IR images.

The growth of the right crack can be observed in the IR images shown in Fig. 11. The Fig. 11(a) shows the first detection experiment after $N = 30\,000$ and Fig. 11(c) shows in detail its crack region. The Fig. 11(b) shows the last detection experiment after $N = 550\,000$ and Fig. 11(d) shows the corresponding zoomed crack region.

The black points represent the crack tips and describe the path of the crack growth during the whole performed experiments.

The growth of the left crack can be observed in the IR images shown in Fig. 12. The Fig. 12(a) shows the first detection experiment after $N = 30\,000$ and Fig. 12(c) shows the corresponding zoomed crack region. The Fig. 12(b) shows the last detection experiment after $N = 550\,000$ and Fig. 12(d) shows the zoomed crack region.

The black points describe the path of the crack growth during the whole fatigue test as well.

Based on the obtained results, the length of the cracks can be estimated as well. From the IR images and measure in the laboratory it has been established that 79.64 pixels correspond to 40 mm. Thus, one pixel corresponds to 0.502 mm.

Two methods were applied to establish the location of the pixel corresponding to the crack tip. The first one considers the pixel corresponding to the highest temperature reached in the IR image. The second one assumes that the temperature at the crack location is above

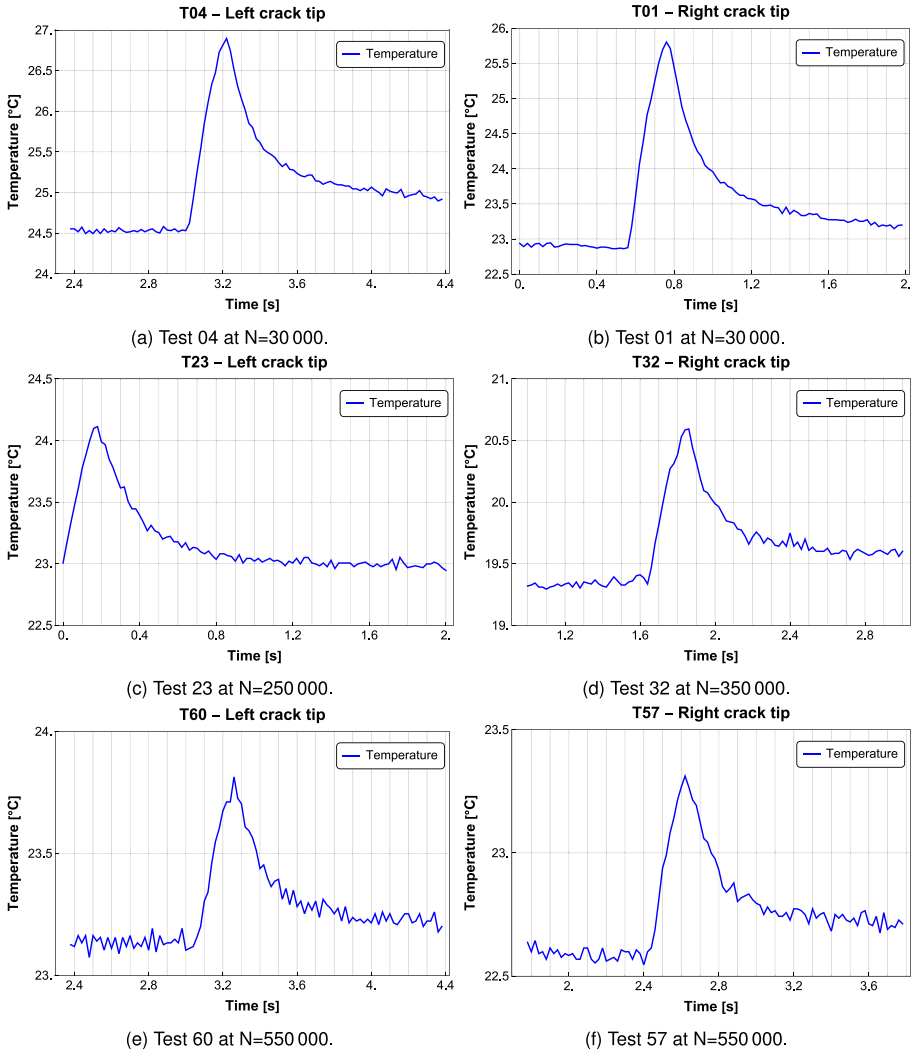

(a) Test 04 at N=30 000. (b) Test 01 at N=30 000.

(c) Test 23 at N=250 000. (d) Test 32 at N=350 000.

(e) Test 60 at N=550 000. (f) Test 57 at N=550 000.

Fig. 10. Temperature evolution of the pixel corresponding to the crack tip.

Table 2
Left side: Location of the crack tip and crack length based on IR images.

Test Nr.	N [–]	X_{l1} [px]	Y_{l1} [px]	L_{l1} [mm]	X_{l2} [px]	Y_{l2} [px]	L_{l2} [mm]	$L_l = 0.5(L_{l1} + L_{l2})$ [mm]
4	30 000	156	104	0.00	156	104	0.00	0.00
6	100 000	152	101	2.67	156	101	4.25	3.46
12	150 000	149	97	5.18	151	97	6.48	5.83
17	200 000	145	96	7.50	148	94	7.60	7.55
23	250 000	143	94	8.92	144	92	9.41	9.16
29	300 000	140	91	10.69	139	90	10.82	10.76
34	350 000	138	89	12.30	137	89	12.63	12.46
40	400 000	135	86	14.26	134	97	14.21	14.24
46	450 000	131	87	16.53	130	85	15.62	16.07
52	500 000	129	85	17.95	128	83	17.43	17.69
60	550 000	127	82	19.41	125	82	19.23	19.32

Table 3
Right side: Location of the crack tip and crack length based on IR images.

Test Nr.	N [–]	X_{r1} [px]	Y_{r1} [px]	L_{r1} [mm]	X_{r2} [px]	Y_{r2} [px]	L_{r2} [mm]	$L_r = 0.5(L_{r1} + L_{r2})$ [mm]
3	30 000	221	144	0.0	220	146	0.00	0.00
5	100 000	231	147	2.62	232	148	3.04	2.83
10	150 000	234	149	4.87	235	149	4.85	4.86
15	200 000	236	150	6.12	237	150	6.65	6.39
21	250 000	238	151	8.37	239	151	8.72	8.54
27	300 000	238	152	10.14	239	152	10.30	10.22
32	350 000	242	154	11.50	242	154	11.88	11.69
38	400 000	244	155	12.85	245	156	14.00	13.42
44	450 000	246	156	14.62	247	157	15.59	15.11
50	500 000	248	158	16.04	249	158	17.00	16.52
57	550 000	250	160	17.51	251	159	17.71	17.61

a certain threshold, which depends on the standard deviation of the temperature in the crack area. Thus, binary IR images were obtained by considering this temperature threshold. Then, the pixel farthest from the coil among the pixels with a higher temperature in threshold was set as the crack tip.

The location of the crack tips and the length increase of both cracks during the cyclic loading are given in Tables 2 and 3. The location given in pixels corresponds to every IR image taken during the crack detection.

As it can be observed in Figs. 14 and 16, the obtained crack paths offer a credible trajectory of the crack growth on both sides. Now in order to see how reliable the obtained results are, it is necessary to compare them with those obtained from microscopic images.

4.2. Results obtained from digital microscope

During the fatigue test, at the same moment as the IR images, digital microscopic pictures of the crack were taken as well. The evolution of

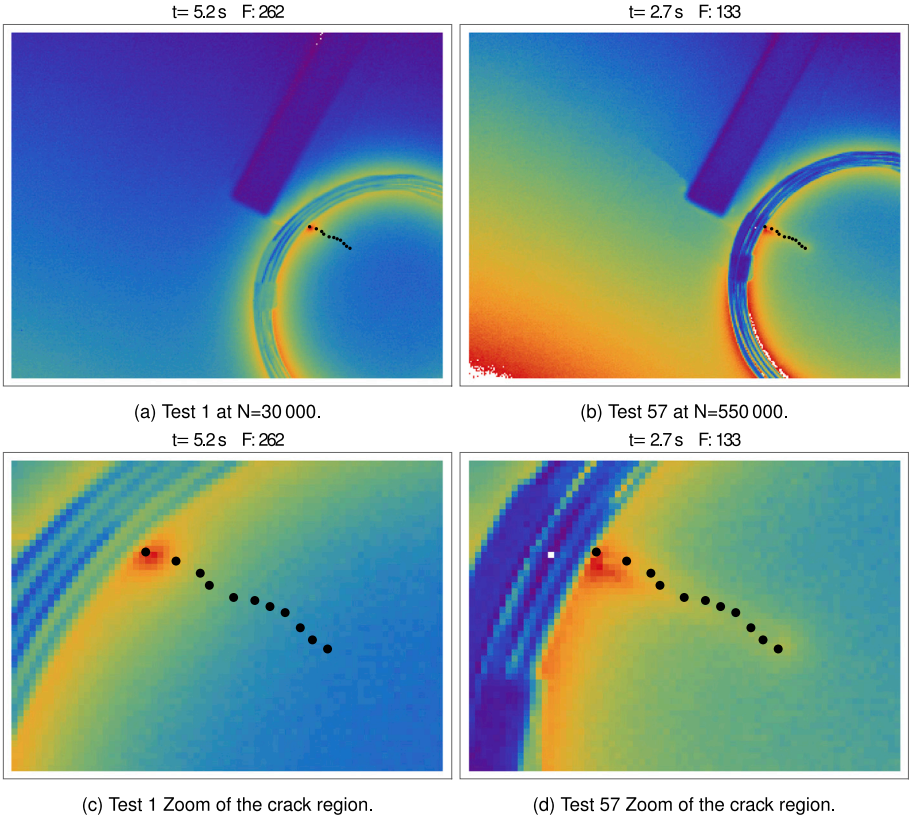

(a) Test 1 at N=30 000. (b) Test 57 at N=550 000.

(c) Test 1 Zoom of the crack region. (d) Test 57 Zoom of the crack region.

Fig. 11. Right crack growth at N = 30 000 and N = 550 000 loading cycles.

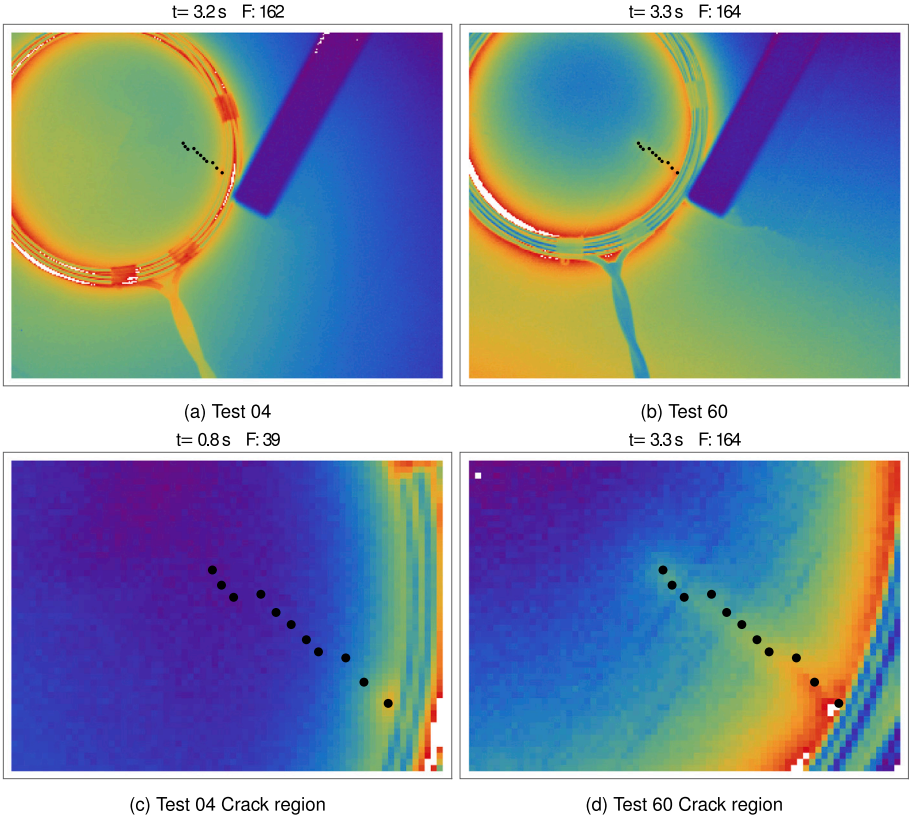

(a) Test 04 (b) Test 60

(c) Test 04 Crack region (d) Test 60 Crack region

Fig. 12. Left crack growth at N = 30 000 and N = 550 000 loading cycles.

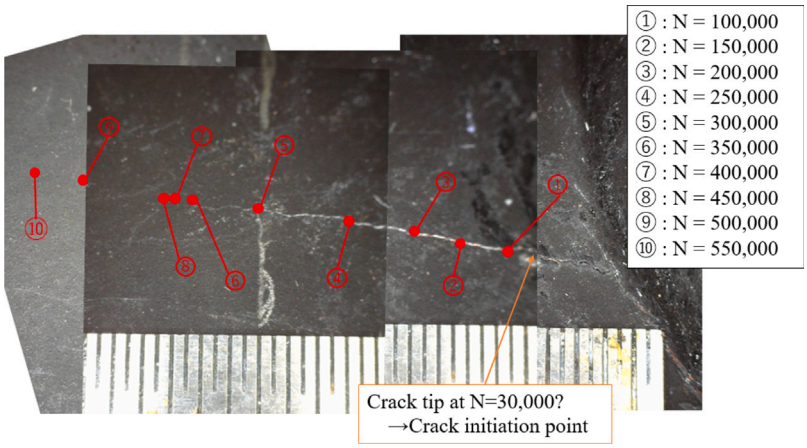

Fig. 13. Left crack picture taken with a digital microscope.

Table 4
Left side: Crack length based on microscopic images and their difference with the results obtained from IR images.

Test Nr.	N [–]	L_{dl} [mm]	$\lvert L_{dl} - L_l \rvert$ [mm]
4	30 000	0.00	0.00
6	100 000	1.17	2.29
12	150 000	2.85	2.98
17	200 000	4.48	3.07
23	250 000	6.74	2.42
29	300 000	9.89	0.87
34	350 000	12.16	0.30
40	400 000	12.79	1.45
46	450 000	13.19	2.89
52	500 000	16.03	1.66
60	550 000	17.71	1.61

Table 5
Right side: Crack lengths based on microscopic images and their difference with the results obtained from IR images.

Test Nr.	N [–]	L_{dr} [mm]	$\lvert L_{dr} - L_r \rvert$ [mm]
3	30 000	0.00	0.00
5	100 000	3.51	0.68
10	150 000	5.35	0.49
15	200 000	6.48	0.09
21	250 000	8.99	0.45
27	300 000	9.67	0.55
32	350 000	12.51	0.82
38	400 000	13.22	0.20
44	450 000	13.32	1.79
50	500 000	14.32	2.20
57	550 000	14.75	2.86

the growth of both cracks can be observed in Figs. 13 and 15 and the corresponding measures are displayed in Tables 4 and 5.

According to these digital pictures, the length of the left crack is 17.71 mm, which means 1,61 mm difference with the value estimated from the IR images. On the other hand, the length of the right crack is 14.75 mm, which means 2.86 mm difference with the value estimated from the IR images.

From the practical point of view, the differences on the left crack is negligible and should not be a cause of concern for monitoring. However, on the right side, the difference cannot be considered as negligible. As a matter of fact, it could be plausible to assume that the position of the real crack opening remains under the coating, so that, it is impossible to observe it with a digital camera. For this reason, the lengths obtained with the microscope are smaller than those obtained from the IR images, see the blue curves in Figs. 14 and 16.

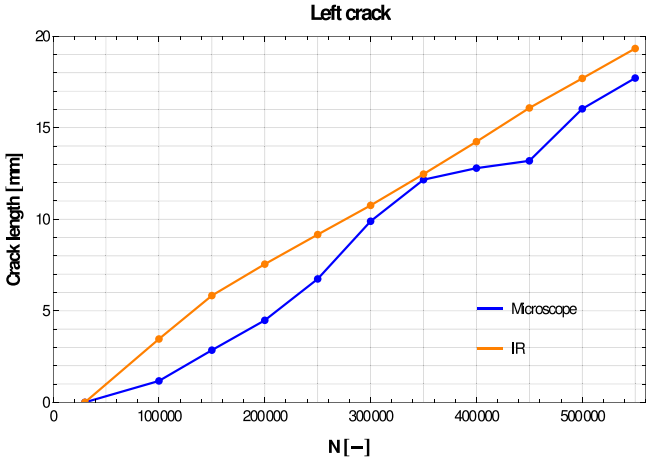

Fig. 14. Left crack: length evolution obtained from IR and microscopic images during the fatigue test.

In order to disclose the cause of this difference, the coating above the right crack tip was removed, see Fig. 17.

As suspected, the real crack length was longer than the observed one on the coating, see Fig. 18. As a matter of fact, the crack tip under the coating was located 1.58 mm beyond the crack tip observed with the microscope, see the orange line in Fig. 18(b). This result means that the real difference between the IR and the microscope length detection of the right crack is indeed 1.28 mm and not 2.86 mm as it is shown in Table 5.

Thus, from the practical point of view we can assure that the IR method offers a reliable and faster alternative to measure the crack length.

4.3. Crack growth rate

By considering the IR images, the crack length evolution as function of the loading cycles for both cracks can be calculated and it is depicted in Fig. 19. As it is observed, the growth of both cracks is almost linear and have almost the same geometry. Based on these facts, we estimate a rate of the crack growth of 3.50 mm per 100 000 cycles.

Similar behaviour has been observed in other specimens, such as, welded specimens from steel JIS-SM490 A and JIS-SM400 A under LCF [15], cruciform joint from steel S355NL [16], fillet welded joints from steel S355 [17] and turbine runner from steel X4CrNiMo16-5-1 [18].

The small differences between the crack lengths estimated from the IR images with those obtained from the microscopic images endorse the reliability of the NDT method proposed for fatigue crack monitoring.

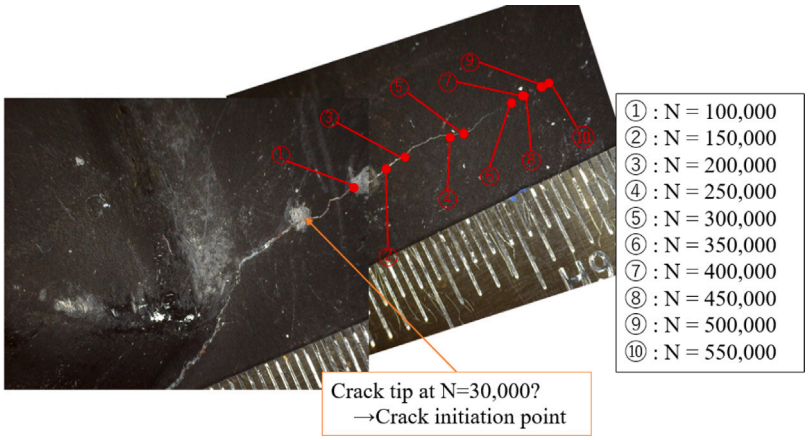

Fig. 15. Right crack picture taken with a digital microscope.

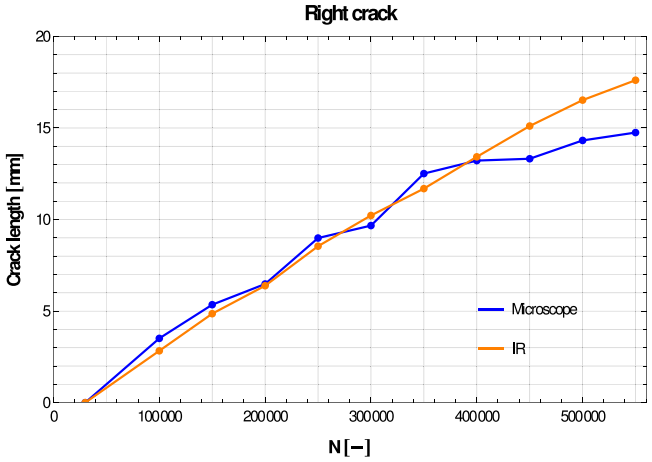

Fig. 16. Right crack: length evolution obtained from IR and microscopic images during the fatigue test.

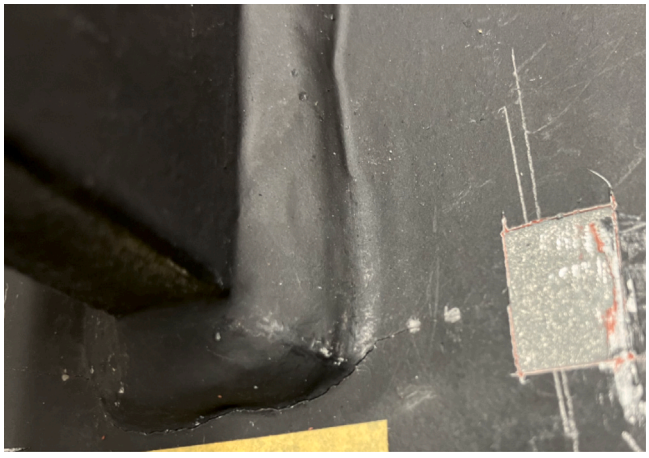

(a) Large view.

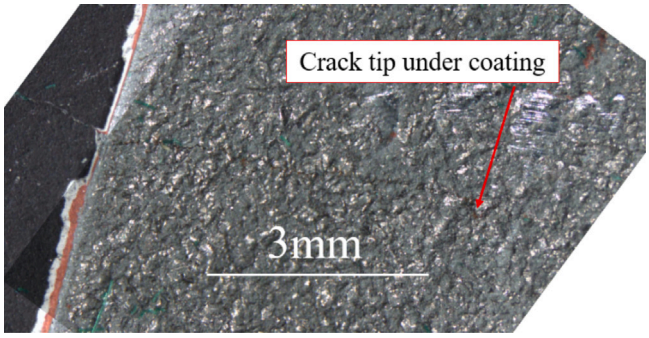

(b) Crack tip region.

Fig. 17. Right crack: Removing of the coating.

5. Conclusions and subsequent research

Performing a reliable crack growth monitoring plays an important role in the steel structures maintenance. In this research, a NDT method based on active thermography was applied to detect in real time the crack presence and to monitor the crack growing in a SM490 steel welded specimen subjected to a cyclic loading. The IR images obtained during the thermal excitation allow to observe the crack tips on the specimen. A limitation of the method used is that the crack tip can be observed once it is not covered by the coil. This implies that the design of the coil must be optimized to be able to observe the crack from its initiation. Once this limitation is overcome, by considering the location of the crack tips, the crack propagation and length during the cyclic loading were established.

The differences on crack length obtained by the thermographical and microscopic methods are negligible and should not be a cause of concern in the inspection of structures.

The obtained results show also that the cracks at both sides of the weld toe have a similar linear growth rate. Moreover, as expected from the theory, the speed of the crack growth and the final crack length are alike as well. It is worth to mentioning, that the crack region was covered with a coating, which did not affect the detection of the crack tips and the corresponding measurements. In fact, after removing the coating on the right crack, it was confirmed that the real crack length was longer than that obtained with the microscope. These facts prove how suitable and reliable the proposed NDT method to detect cracks in large steel structures is.

Since the used crack detection system is portable and lightweight, it is suitable for inspecting and monitoring large steel structures on site. This represents a great potential in the monitoring of crack initiation and propagation on bridges, offshore oil installations, railroad rails, wind energy towers, and other structures. The corresponding costs can thus be reduced considerably.

Despite the promising results, there are still some facts, which must be considered in future investigations, such as thickness of the coating, effect of the applied stress on the crack growth rate and the effect of stress ratio.

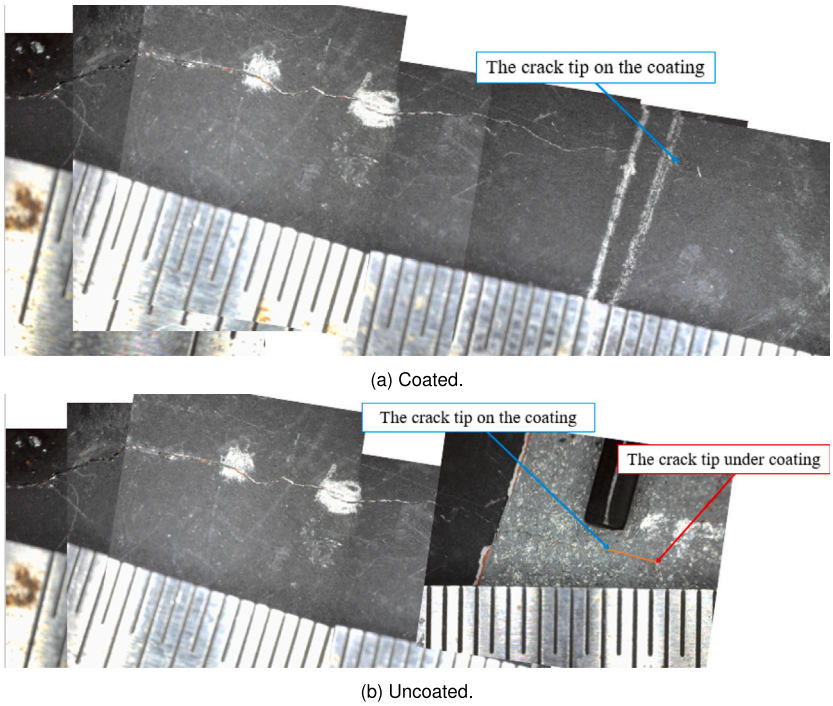

Fig. 18. Right crack: Crack tip location on the coated plate before and after removing the coating.

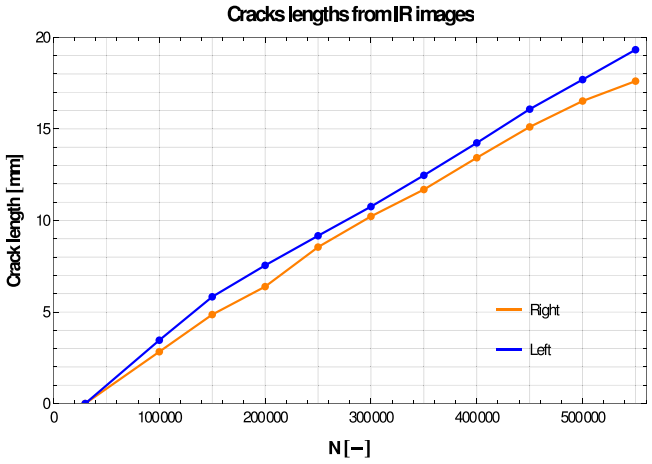

Fig. 19. Crack length evolution of both cracks during the cyclic loading.

CRediT authorship contribution statement

Paul Dario Toasa Caiza: Writing – original draft, Methodology, Investigation, Conceptualization. **Daiki Shiozawa:** Validation, Methodology, Investigation. **Yuya Murao:** Investigation. **Thomas Ummenhofer:** Validation. **Takahide Sakagami:** Investigation.

Declaration of competing interest

The authors declare the following financial interests/personal relationships which may be considered as potential competing interests: Paul Dario TOASA CAIZA reports administrative support was provided by Karlsruhe Institute of Technology. If there are other authors, they declare that they have no known competing financial interests or personal relationships that could have appeared to influence the work reported in this paper.

Acknowledgments

The authors want to express their gratitude to the German Research Foundation (DFG[3]) for the funds granted to perform this research between Germany and Japan. Project Number: 519180280.

Data availability

Data will be made available on request.

References

[1] Thatcher J, Crump D, Devivier C, Bailey P, Dulieu-Barton J. Low cost infrared thermography for automated crack monitoring in fatigue testing. Opt Lasers Eng 2020;126:105914. http://dx.doi.org/10.1016/j.optlaseng.2019.105914.
[2] Bercelli L, Levieil B, Doudard C, Malek B, Bridier F, Ezanno A. Use of infrared thermography to model the effective stress ratio effect on fatigue crack growth in welded T-joints. Eng Fract Mech 2023;279:109061. http://dx.doi.org/10.1016/j.engfracmech.2023.109061.
[3] Boussattine Z, Ranc N, Palin-Luc T. About the heat sources generated during fatigue crack growth: What consequences on the stress intensity factor? Theor Appl Fract Mech 2020;109:102704. http://dx.doi.org/10.1016/j.tafmec.2020.102704.
[4] Hajshirmohammadi B, Khonsari M. A simple approach for predicting fatigue crack propagation rate based on thermography. Theor Appl Fract Mech 2020;107:102534. http://dx.doi.org/10.1016/j.tafmec.2020.102534.
[5] Schweda M, Beck T, Offermann M, Singheiser L. Thermographic analysis and modelling of the delamination crack growth in a thermal barrier coating on Fecralloy substrate. Surf Coat Technol 2013;217:124–8. http://dx.doi.org/10.1016/j.surfcoat.2012.12.002.
[6] Sakagami T. Remote nondestructive evaluation technique using infrared thermography for fatigue cracks in steel bridges. Fatigue Fract Eng Mater Struct 2015;38(7):755–79. http://dx.doi.org/10.1111/ffe.12302.
[7] Netzelmann U, Walle G, Lugin S, Ehlen A, Bessert S, Valeske B. Induction thermography: principle, applications and first steps towards standardisation. Quant InfraRed Thermogr J 2016;13(2):170–81. http://dx.doi.org/10.1080/17686733.2016.1145842.
[8] Oswald-Tranta B. Detection and characterisation of short fatigue cracks by inductive thermography. Quant InfraRed Thermogr J 2022;19(4):239–60. http://dx.doi.org/10.1080/17686733.2021.1953226.

[3] Deutsche Forschungsgemeinschaft

[9] Toasa Caiza PD, Schwendemann R, Calero P, Ummenhofer T. Portable generator to detect cracks on large steel structures: An application of inductive thermography. J Nondestruct Eval 2021;40(63):1–11. http://dx.doi.org/10.1007/s10921-021-00795-5.

[10] Toasa Caiza PD, Shiozawa D, Ummenhofer T, Sakagami T. Real time detection of fatigue cracks on steel structures by applying square wave induction. Eng Fail Anal 2024;166:108799. http://dx.doi.org/10.1016/j.engfailanal.2024.108799.

[11] Mikulski Z, Lassen T. Fatigue crack initiation and subsequent crack growth in fillet welded steel joints. Int J Fatigue 2019;120:303–18. http://dx.doi.org/10.1016/j.ijfatigue.2018.11.014.

[12] Budynas RG, Nisbett KJ. Shigley's mechanical engineering design. 9th ed.. McGraw-Hill Science/Engineering/Math; 2010.

[13] Schwendemann R, Decker S, Hiller M, Braun M. A Modular Converter- and Signal-Processing-Platform for Academic Research in the Field of Power Electronics. In: 2018 international power electronics conference (IPEC-niigata 2018 -ECCE Asia). 2018, p. 3074–80. http://dx.doi.org/10.23919/IPEC.2018.8507630.

[14] Trausch I. Entwurf und inbetriebnahme einer MOSFET H-brückenschaltung für eine zerstörungsfreie werkstoffprüfung (B.Sc. Thesis), Intitute of Electrical Engineering (ETI). Karlsruhe Institute of Technology (KIT); 2019.

[15] Hanji T, Tateishi K, Terao N, Shimizu M. Fatigue crack growth prediction of welded joints in low-cycle fatigue region. Weld World 2017;61:1189–97. http://dx.doi.org/10.1007/s40194-017-0504-3.

[16] Tchoffo Ngoula D, Beier H, Vormwald M. Fatigue crack growth in cruciform welded joints: Influence of residual stresses and of the weld toe geometry. Int J Fatigue 2017;101:253–62. http://dx.doi.org/10.1016/j.ijfatigue.2016.09.020, Fatigue Assessment of Welded Joints by Modern Concepts.

[17] Lewandowski J, Rozumek D. Cracks growth in S355 steel under cyclic bending with fillet welded joint. Theor Appl Fract Mech 2016;86:342–50. http://dx.doi.org/10.1016/j.tafmec.2016.09.003.

[18] Carpinteri A, Brighenti R, Huth H-J, Vantadori S. Fatigue growth of a surface crack in a welded T-joint. Int J Fatigue 2005;27(1):59–69. http://dx.doi.org/10.1016/j.ijfatigue.2004.05.007.